Optics EXPRESS

Raman-shifted wavelength-selectable pulsed fiber laser with high repetition rate and high pulse energy in the visible

L. Xu,* S. Alam, Q. Kang, D. P. Shepherd, and D. J. Richardson

Optoelectronics Research Centre, University of Southampton, Southampton, SO17 1BJ, UK
*l.xu@soton.ac.uk

Abstract: A high-pulse-energy, diffraction-limited, wavelength-selectable, visible source, based on Raman frequency shifting of a frequency-doubled Yb-doped fiber laser, has been studied. The relative length-scaling laws of Raman gain and self-phase modulation push the design towards short fiber lengths with large core size. It is experimentally demonstrated that the Raman clean-up effect in a graded-index multi-mode fiber is not sufficient to obtain diffraction-limited beam quality in the short fiber length. Thus, a large-core photonic crystal fiber is used to maintain diffraction-limited performance and output pulse energies of ~1 μJ, at a 1-MHz repetition rate and 1.3-ns pulse-width are successfully achieved. This step-tunable visible source should find applications in photoacoustic microscopy.

Published by The Optical Society under the terms of the Creative Commons Attribution 4.0 License. Further distribution of this work must maintain attribution to the author(s) and the published article's title, journal citation, and DOI.

OCIS codes: (140.3510) Lasers, fiber; (140.3538) Lasers, pulsed; (140.3550) Lasers, Raman.

References and links

1. J. Yao, L. Wang, J. M. Yang, K. I. Maslov, T. T. W. Wong, L. Li, C. H. Huang, J. Zou, and L. V. Wang, "High-speed label-free functional photoacoustic microscopy of mouse brain in action," Nat. Methods **12**(5), 407–410 (2015).
2. A. Rosencwaig and G. Busse, "High-resolution photoacoustic thermal-wave microscopy," Appl. Phys. Lett. **36**(9), 725–727 (1980).
3. L. V. Wang and S. Hu, "Photoacoustic tomography: in vivo imaging from organelles to organs," Science **335**(6075), 1458–1462 (2012).
4. K. Maslov, H. F. Zhang, S. Hu, and L. V. Wang, "Optical-resolution photoacoustic microscopy for in vivo imaging of single capillaries," Opt. Lett. **33**(9), 929–931 (2008).
5. K. Pu, A. J. Shuhendler, J. V. Jokerst, J. Mei, S. S. Gambhir, Z. Bao, and J. Rao, "Semiconducting polymer nanoparticles as photoacoustic molecular imaging probes in living mice," Nat. Nanotechnol. **9**(3), 233–239 (2014).
6. J. Bertolotti, E. G. van Putten, C. Blum, A. Lagendijk, W. L. Vos, and A. P. Mosk, "Non-invasive imaging through opaque scattering layers," Nature **491**(7423), 232–234 (2012).
7. T. J. Allen, M. O. Berendt, J. Spurrell, S. U. Alam, E. Z. Zhang, D. J. Richardson, and P. C. Beard, "Novel fibre lasers as excitation sources for photoacoustic tomography and microscopy," in *SPIE PHOTONICS WEST* (2016), pp. 97080–97085.
8. P. Hajireza, A. Forbrich, and R. Zemp, "In-Vivo functional optical-resolution photoacoustic microscopy with stimulated Raman scattering fiber-laser source," Biomed. Opt. Express **5**(2), 539–546 (2014).
9. A. Loya, J. P. Dumas, and T. Buma, "Photoacoustic microscopy with a tunable source based on cascaded stimulated Raman scattering in a large-mode area photonic crystal fiber," in *Proceedings of IEEE Ultrasonics Symposium* (2012).
10. K. K. Chen, S. U. Alam, P. Horak, C. A. Codemard, A. Malinowski, and D. J. Richardson, "Excitation of individual Raman Stokes lines in the visible regime using rectangular-shaped nanosecond optical pulses at 530 nm," Opt. Lett. **35**(14), 2433–2435 (2010).
11. K. T. Vu, A. Malinowski, D. J. Richardson, F. Ghiringhelli, L. M. B. Hickey, and M. N. Zervas, "Adaptive pulse shape control in a diode-seeded nanosecond fiber MOPA system," Opt. Express **14**(23), 10996–11001 (2006).
12. G. L. Lan, P. K. Banerjee, and S. S. Mitra, "Raman scattering in optical fibers," J. Raman Spectrosc. **11**(5), 416–423 (1981).
13. N. B. Terry, T. G. Alley, and T. H. Russell, "An explanation of SRS beam cleanup in graded-index fibers and the absence of SRS beam cleanup in step-index fibers," Opt. Express **15**(26), 17509–17519 (2007).
14. J. Cheng, M. E. V. Pedersen, K. Charan, K. Wang, C. Xu, L. Grüner-Nielsen, and D. Jakobsen, "Intermodal four-wave mixing in a higher-order-mode fiber," Appl. Phys. Lett. **101**(16), 161106 (2012).

#278754 http://dx.doi.org/10.1364/OE.25.000351
Journal © 2017 Received 13 Oct 2016; revised 22 Nov 2016; accepted 23 Nov 2016; published 5 Jan 2017

Optics EXPRESS

15. L. G. Wright, D. N. Christodoulides, and F. W. Wise, "Controllable spatiotemporal nonlinear effects in multimode fibres," Nat. Photonics **9**(5), 306–310 (2015).
16. C. Antonelli, M. Shtaif, and A. Mecozzi, "Modeling of nonlinear propagation in space-division multiplexed fiber-optic transmission," J. Lightwave Technol. **34**(1), 36–54 (2016).
17. Y. Xiao, R.-J. Essiambre, M. Desgroseilliers, A. M. Tulino, R. Ryf, S. Mumtaz, and G. P. Agrawal, "Theory of intermodal four-wave mixing with random linear mode coupling in few-mode fibers," Opt. Express **22**(26), 32039–32059 (2014).
18. R. J. Essiambre, M. A. Mestre, R. Ryf, A. H. Gnauck, R. W. Tkach, A. R. Chraplyvy, Y. Sun, X. Jiang, and R. Lingle, "Experimental Investigation of Inter-Modal Four-Wave Mixing in Few-Mode Fibers," IEEE Photonics Technol. Lett. **25**(6), 539–542 (2013).

1. Introduction

Photoacoustic microscopy (PAM) is an emerging technology that offers unprecedented high-contrast imaging based on physiological differences in tissue optical absorption [1–3]. In particular, optical-resolution photoacoustic microscopy (OR-PAM) is capable of achieving optical-absorption-contrast imaging with micron-scale resolution [4–6], by enabling acoustic detection of thermoelastically induced pressure waves from biomolecules with the absorption of short-pulsed light. For OR-PAM, pulsed lasers with μJ-level energies, good beam quality and excitation wavelengths in the visible and near-infrared are generally required. Compared to bulk laser and dye laser sources, fiber laser technology offers the prospect of compact, reliable and efficient photoacoustic excitation sources for clinical use. In addition, fiber lasers can provide high pulse-repetition frequencies to achieve rapid image acquisition. In our previous work, a frequency-doubled pulsed-fiber-laser excitation source with 1-MHz repetition rate has shown a capability of acquisition of 2×10^6 A-lines per second [7]. However, the fixed wavelength of the laser source imposed severe limitations on the spectroscopic applications.

Cascaded stimulated Raman scattering (SRS) in optical fibers provides a convenient and practical mechanism to increase the number of excitation wavelengths for functional photoacoustic microscopy [8, 9]. However, in this scheme all the subsequent Stokes lines are excited simultaneously and therefore the energy transfer efficiency from pump to the desired Stokes line is compromised. Furthermore additional spectral filtering is required to select an individual line. Selective excitation of Raman Stokes wavelengths can be realized by using a flat-topped rectangular pump pulse, since all points across the pulse experience identical Raman gain. Using this concept, selective excitation of individual Raman Stokes lines of up to the ninth order has been reported previously by our group [10]. However, it was found that with increased pump peak power, the suppression ratio of each excited Stokes line decreased and also the spectral bandwidths of the Stokes lines were broadened by other nonlinear effects. The resulting energy spectral density due to the distribution of competing energy over a wide spectral range is thus reduced.

Here we report an investigation of selective generation of high-pulse-energy Raman Stokes lines by cascaded SRS in a number of different fiber geometries. By choosing large-mode-area (LMA) photonic crystal fiber (PCF), ~1-μJ energy, 1-MHz repetition rate, 1.3-ns pulses with single-mode beam quality and relatively narrow spectral bandwidth have been achieved at the Raman Stokes wavelengths of 560 nm (2nd Stokes) and 575 nm (3rd Stokes), when pumped by a frequency-doubled Yb-doped-fiber master oscillator power amplifier (MOPA) system. These wavelengths are targeted as they are located in the absorption spectra of oxy and deoxy haemoglobin.

2. Experiment

A schematic of the tunable source is shown in Fig. 1. The nanosecond master-oscillator-power-amplifier (MOPA) consisted of a continuous-wave (CW) polarization-maintaining (PM)-fiber-pigtailed tunable diode laser as the seed, followed by a 5-stage Yb-doped fiber-amplifier chain. An electro-optic modulator (EOM) was used after the first pre-amplifier to slice the amplified CW radiation into a pulsed format. The EOM was driven by an arbitrary

Optics EXPRESS

waveform generator (AWG) with a tunable repetition rate and pulse duration. The first and second amplifiers had 3-m-long fibers (Nufern PM-YDF-5/130) and were core-pumped by 975 nm single-mode laser diodes, and the same gain fiber was used in the third amplifier stage but was cladding-pumped in this instance. An acoustic-optic modulator (AOM) was inserted after the third amplifier in order to eliminate the amplified spontaneous emission (ASE) between pulses and also to increase the dynamic extinction ratio between the amplified pulses. However, due to the average power handling capabilities of the AOM, the output power from the third amplifier was set not to exceed 200 mW. The fourth amplifier had a 3-m-long Yb-doped fiber (Nufern PLMA-YDF-10/125-VIII) with a 10 μm diameter core and was cladding-pumped. The cladding-pumped final-stage power amplifier comprised LMA Yb-doped fiber (PLMA-YDF-25/250-VIII) with a core diameter of 25 μm and a length of 4 meters.

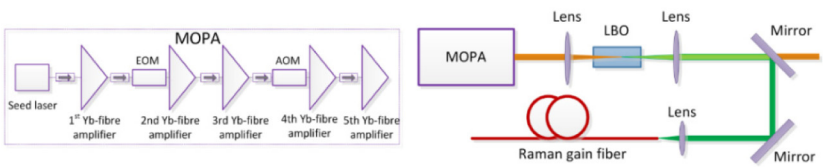

Fig. 1. Schematic of the experimental setup.

The MOPA was operated at an output wavelength of 1064 nm, such that frequency-doubling and Raman-shifting would deliver our targeted wavelengths. The collimated beam of the output from the MOPA was focused into a lithium triborate (LBO) nonlinear crystal for second harmonic generation (SHG). The LBO was cut with an angle of θ = 90° and φ = 0° in order to realize type-I noncritical phase-matching and avoid spatial walk-off. The LBO has a length of 25 mm and was held in an oven with the temperature set at 149 °C. Both the entrance and exit surfaces of the LBO were anti-reflection (AR) coated at 1064nm and 532nm. The generated second harmonic beam was collimated and separated from the residual fundamental beam after reflection from dichroic mirrors. The second harmonic beam was then focussed by an aspheric lens into a Raman gain fiber to frequency shift it to the targeted wavelengths.

3. Results and discussion

The repetition rate of the MOPA system was set at 1 MHz and 1.3-ns pulses with a rectangular shape were obtained by shaping the RF signal from the AWG (temporal resolution of <0.1 ns) to compensate for the gain saturation effects in the fiber amplifiers [11]. The fundamental-mode output beam (M^2 < 1.1) had an average power of 18 W and a narrow spectral linewidth of <0.05 nm (measurement limited by the resolution of the optical spectrum analyzer ANDO AQ6315). After passing through the LBO crystal, a maximum of 11.8-W average power was achieved at a wavelength of 532-nm wavelength. The corresponding conversion efficiency reached 65%, as shown in Fig. 2.

The green light was then launched into various passive fibers with different geometries to assess their ability to generate Raman Stokes lines of sufficient spectral energy density and good beam quality. Firstly, we tested a step-index single-mode fiber (SMF) (S405-XP, Thorlabs), which had a pure silica core to avoid any possibility of photo-darkening due to the intense visible light. The fiber core had a diameter of 4 μm and a cut-off wavelength of 380 nm. With increasing pump power, successive frequency down-shifted Stokes pulses were generated. The wavelength peaks of the 1st, 2nd and 3rd Stokes were at 546 nm, 560nm and 575 nm, respectively, corresponding to the expected 13.2-THz Raman frequency shift in silica [12]. By using a 15-meter length of SMF, the optimized, selectively excited, Raman Stokes lines exhibited a good suppression ratio of more than 10 dB in comparison to adjacent peak spectral as shown in Fig. 3(a). The different coloured lines represent the output spectra of different selectively excited Raman Stokes orders, through use of different launched pump

Optics EXPRESS

powers. The power transfer efficiencies from the pump to the three Stokes lines were 91% (blue spectrum), 87% (green spectrum) and 70% (red spectrum) for the 1st, 2nd and 3rd Stokes lines, respectively. The spectral components had linewidths (3 dB) of 1.8 nm, 2.6 nm and 3.3 nm for the 1st, 2nd and 3rd order Stokes, respectively. The calculated pulse energies within the 3-dB bandwidth were 0.2 μJ for the 1st Stokes line and 0.5 μJ for the other two Stokes lines. Any further increase in input power would have depleted the 3rd Stokes pulse and shifted the output to longer wavelengths not required for our particular application. In an attempt to achieve higher pulse energies at the targeted 2nd and 3rd Stokes wavelengths, we shortened the fiber length and increased the input pulse energy. For a 5-meter-long SMF, the 2nd and 3rd Stokes spectra were then significantly broadened in comparison to that obtained with the longer fiber, as shown in Fig. 3.

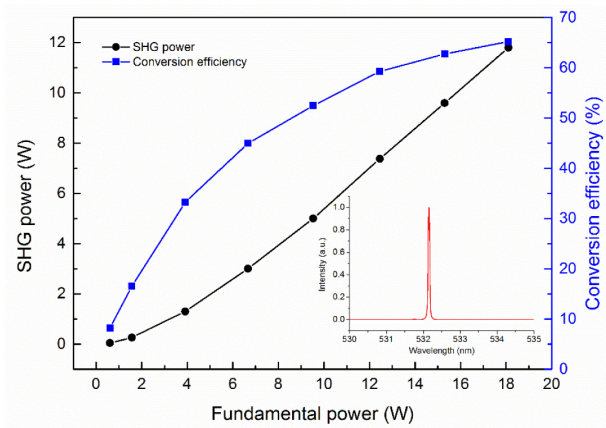

Fig. 2. SHG power and conversion efficiency versus input fundamental power. The inset shows the second harmonic spectrum.

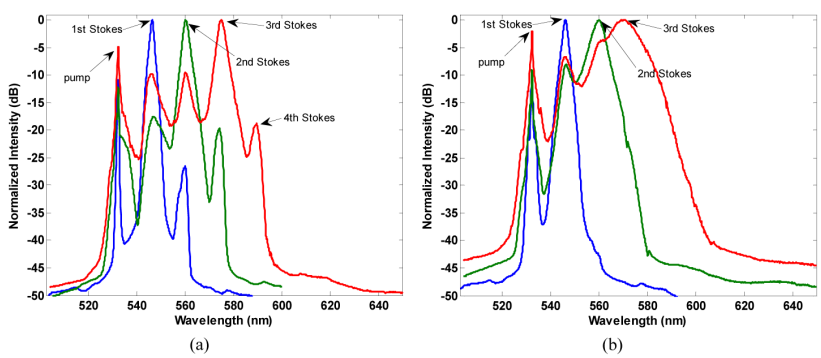

Fig. 3. Output Raman spectra from a step-index single mode fiber with lengths of 15 m (a) and 5 m (b). The different colours represent different pump powers launched into the fibers to selectively excite different Stokes lines. Pump power: blue 285 mW; green 685 mW; red 880 mW in (a) and blue 540 mW; green 1.3 W; red 1.5 W in (b).

The 3-dB bandwidth of the 2nd and 3rd Stokes spectra were increased to 5.7 nm and 12.3 nm, respectively, containing pulse energies of 0.9 μJ and 1.0 μJ, significantly reducing the spectral energy density. The SRS line broadening is thought to be due to self-phase modulation (SPM) because of the increased pulse intensity. The SPM gives rise to an intensity-dependent phase shift $\varnothing = \gamma P_0 L_{eff}$, where γ is the fiber nonlinear parameter, P_0 is the pulse peak power and L_{eff} is the effective fiber length. The variation of the phase shift, which is associated with the leading and trailing edges of the rectangular pulse, induces a

Optics EXPRESS

frequency chirp (spectral broadening) . $\delta\omega(t)=\frac{d\varnothing}{dt}$ The Raman gain G is given by $G=\frac{P_{out}}{P_{in}}=\exp(\frac{g_R P_0 L_{eff}}{A_{eff}}-\alpha L)$, where P_{in}, P_{out} are the input and output power of the Raman from the fiber, g_R is the fiber Raman gain coefficient, A_{eff} is the fiber effective core area, α is the fiber loss and L is the real fiber length. Since the peak non-linear phase shift of SPM has a linear dependency on fiber length, while the Raman gain has an exponential dependency, the use of a shorter fiber length and higher pulse energy has led to an increase in the relative impact of SPM on the output spectrum.

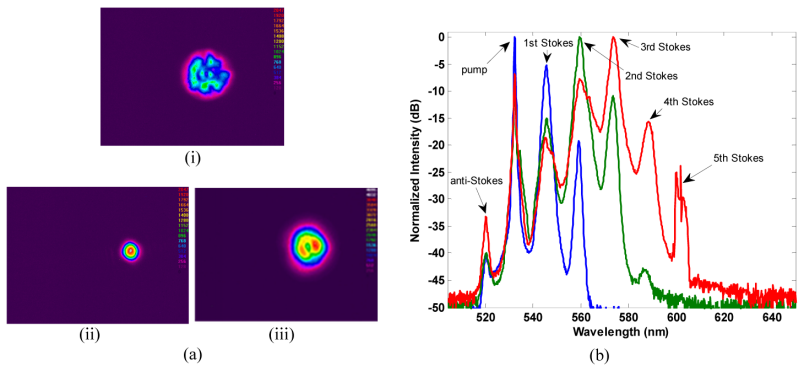

Fig. 4. (a) Output beam profiles from graded-index fiber: pump after 200 m fiber (i); 3rd Stokes after 200 m fiber (ii); 3rd Stokes after 19 m fiber (iii) and (b) Raman spectra of the 19 m graded-index fiber. In (b) the different colours represent different pump powers launched into the fibers to selectively excite different Stokes lines. Pump power: blue 890 mW; green 1.1 W; red 1.5 W.

Considering the length-scaling rules of SPM versus Raman scattering, an increase in the fiber core size rather than reduction in the fiber length was considered to be a more promising way to scale the Stokes pulse energy. We therefore used a large core (~17 μm) graded-index multi-mode fiber (GIMMF), as it has been shown that a graded-index profile can lead to SRS beam clean-up in multi-mode fibers due to the lower-order transverse Stokes modes experiencing more gain than the higher-order transverse Stokes modes [13]. Hence, we hoped to be able to obtain fundamental-mode beam quality, while avoiding SPM-induced spectral broadening. We observed the clean-up effect in an experiment with a 200-m long GIMMF, where the Raman Stokes output beam was found to be in the fundamental mode despite the pump being highly multi-moded. When the pump power was set to be lower than the Raman threshold and there was no Raman generated in the 200 m long GIMMF, the output beam of the pump was highly multi-moded due to the large core, as shown in Fig. 3(a, i). Increasing pump power led to the generation of Raman Stokes pulses and a narrow band-pass filter was then used to filter out the 3rd Stokes wave. It can be seen from the Fig. 3(a, ii) that the filtered Stokes beam is in the fundamental mode for the 200-m length fiber. However, the pulse energy in the selectively excited 3rd Stokes is very low for such a long length of fiber. A shorter length of fiber (19 m) was then used for selectively exciting Stokes lines of up to 3rd order with high pulse energy. Due to the larger core size, the 3-dB bandwidths of the Stokes-shifted components in the GIMMF were indeed narrowed to 2.3 nm and 2.7 nm for the central wavelengths of 560 nm and 575 nm. However, as shown in Fig. 3(a, iii), the Stokes output beam was no longer in a clean fundamental mode. This is thought to be due to several possible effects: (i) a reduced Raman beam clean-up effect in the shorter length fiber, (ii) an observed degradation in the beam quality of the SHG pump beam at higher powers, and (iii) greater nonlinear phase-matched inter-modal coupling. The behaviour of inter-modal

Optics EXPRESS

nonlinear interactions has been investigated and reported both experimentally and theoretically [14–18]. It can be seen that the output spectrum when optimised for the 3rd Stokes in the GIMMF (red line in Fig. 4) has extra spectral features in comparison to that for the SMF (Fig. 3). We can see a more evident 5th Stokes and an anti-Stokes line at 520 nm. This is thought to be due to an inter-modal four-wave-mixing (FWM) effect in the GIMMF [14].

Photonic crystal fibers (PCFs) can be designed with a large core surrounded by a cladding consisting of a periodic structure that can produce remarkable optical properties, such as endlessly single-mode operation. Therefore, in order to simultaneously obtain diffraction-limited beam quality, μJ pulse energies, and relatively narrow linewidths for the Raman shifted output, we used an endlessly single-mode PCF, with a core diameter of 10 μm (LMA-10, NKT). For a PCF length of 15 m, selectively excited narrow-spectral-bandwidth Raman Stokes beams, with fundamental-mode beam quality and high pulse energies, were finally successfully achieved. The 3-dB bandwidth of the 2nd and 3rd order Stokes spectral components were 2.9 nm and 3.5 nm, respectively, and the corresponding pulse energies were 1.0 μJ and 0.9 μJ. Figure 5 shows the output Raman spectra and beam profile of the PCF and temporal pulse shapes of the pump and Raman Stokes pulses. The maintenance in rectangular pulse shapes of the Stokes from the pump shows the capability of selective excitation of Raman Stokes wavelengths by using a flat-topped pump pulse.

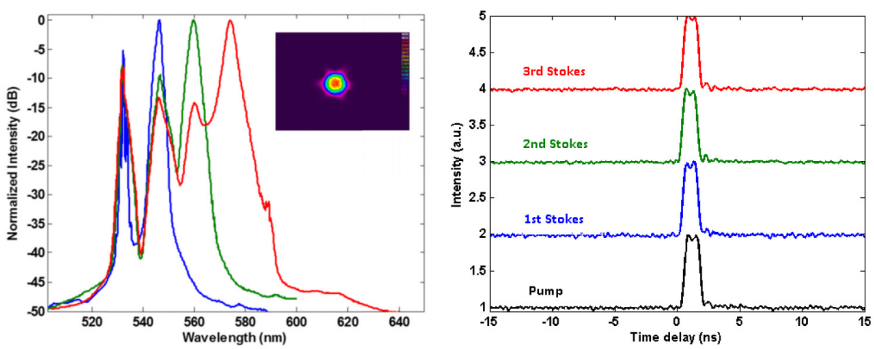

(a) (b)

Fig. 5. (a)Output Raman spectra and beam profile of the 15-m PCF and (b) Pulse shapes of pump and Raman Stokes, all pulse amplitudes are normalized and equally offset for better visibility. In (a) the different colours represent different pump powers launched into the fibers to selectively excite different Stokes lines. Pump power: blue 640 mW; green 1.6 W; red 1.9 W.

4. Conclusion

In conclusion, we have investigated and demonstrated fiber laser sources of discrete Raman-shifted wavelengths with high pulse energy and good beam quality. We have shown that the length scaling laws of the Raman gain and SPM dictate the use of larger core fibers. We also show that the Raman clean-up effect in graded-index multi-mode fiber is not sufficient to obtain diffraction-limited beam quality in the short lengths of fiber required to obtain the targeted high pulse energies. By using a PCF, a wavelength-selective fiber laser source with diffraction-limited output beam with ~1-μJ pulse energy at 1-MHz repetition rate was obtained. The final source has the desired parameters for OR-PAM applications with fast acquisition speed.

Acknowledgments

This work was supported by the UK EPSRC under grant EP/J021970/1. The data are available through the University of Southampton research depository (doi.org/10.5258/SOTON/401326)